Computational Aerodynamics of Oscillating Cascades with the Evolution of Stall

F. Sisto,* Wenquan Wu,† S. Thangam,‡ and S. Jonnavithula§
Stevens Institute of Technology, Hoboken, New Jersey

The applicability of the vortex method to cascades of oscillating airfoils is assessed by computing the unsteady incompressible lift, drag, and moment for small incidence, thickness, and vibratory displacement—the so-called "classical" case. The results for a limited sampling of cascade geometries, reduced frequencies, vibration amplitudes, and interblade phase angles are in excellent agreement with available analytical results. Instantaneous streamline patterns and discretized vorticity distributions are presented as an aid in physical understanding. The importance of the interblade phase angle as a governing parameter is confirmed. Then the effects of mean incidence, vibration amplitude, and stagger angle are studied. Important new results are presented showing the evolution of the classical reactions into the stalled-flow reactions with incidence, frequency, and amplitude as parameters. In particular, the complicated interaction is demonstrated between the structural frequency of the blades (considered as one of the "inputs" to a nonlinear aeroelastic system) and the output frequency spectrum of the aerodynamic reactions. The implications for future direction of research and design code implementation are discussed.

Nomenclature

A = amplitude
A_d = $|C_d|$
A_ℓ = $|C_\ell|$
c = chord length
C_d = drag coefficient, $F_d/(\pi\rho U_\infty cq) = A_d \exp(i\phi)$
C_ℓ = lift coefficient, $F_\ell/(\pi\rho U_\infty cq) = A_\ell \exp(i\phi)$
C_M = moment coefficient, $M/(\pi\rho U_\infty c^2 q)$
f = frequency of vibration, Hz
F = aerodynamic force on blade
h = bending amplitude
K = reduced frequency, $\pi fc/U_\infty$
m = blade order in flow period
n = normal vector of the surface of blade
N = number of vortices
p = spatial periodicity of the array of vortices
q = translation velocity of blade due to vibration
R = area of the solid region
s = coordinate parallel to the blades
t = time
U_∞ = upstream approach velocity
V = velocity
x,y = coordinates of the airfoil
z = complex variable $x + iy$
α = inlet flow angle
β = intrablade phase angle
Γ = circulation
ζ = stagger angle of the blade
θ = torsional displacement
ν = kinematic viscosity
ξ = core radius of the vortices
ρ = density
σ = interblade phase angle
ϕ = phase angle between the force and velocity of blade
ψ = stream function
ω = vorticity
Ω = angular velocity

Subscripts and Superscripts

0 = without vibration
b = blade
d = drag
ℓ = lift
m = solid region
M = moment
t = instantaneous value at time t

Operators

∂ = partial derivatives in compact notation (e.g., $\partial_x = \partial/\partial x$, $\partial_t = \partial/\partial t$, etc.)
∇ = gradient operator $(= i\partial_x + j\partial_y)$
D_t = material derivative $(= \partial_t + \boldsymbol{u} \cdot \nabla)$

Introduction

STALL flutter has been a major obstacle in the design of the fan and compressor components of advanced gas turbine engines. Many theoretical and experimental studies have attempted to illuminate the mechanism of unsteady stall, but it remains a challenging problem.

The important design requirement of predicting analytically the stall flutter characteristics of axial compressor and/or fan blades has long been frustrated by the inability to formulate the unsteady aerodynamic problem in a quantitatively reliable manner. With the development of the vortex method[1,2] and its application here to cascaded airfoils in phased vibratory motion, this limitation seems now to be yielding to computational analysis.

From the viewpoint of numerical calculation, the finite-difference method and finite-element method are very well known and appear to be capable of treating unsteady flow with large separation. Unfortunately, as a rule, the difficulty

Received April 28, 1987; presented as Paper 87-2055 at the AIAA/SAE/ASME/ASEE 23th Joint Propulsion Conference, San Diego, CA, June 29-July 2, 1987; revision received April 18, 1988.

*George Meade Bond Professor, Department of Mechanical Engineering. Associate Fellow AIAA.

†Visiting Professor, Department of Mechanical Engineering, from the Institute of Engineering Thermophysics, Beijing.

‡Associate Professor, Department of Mechanical Engineering. Member AIAA.

§Graduate Student, Department of Mechanical Engineering. Student Member AIAA.

of using Navier-Stokes solvers increases with the Reynolds number. Since a very fine mesh is needed at the high Reynolds numbers of interest in engineering applications, several serious problems arise, such as the requirement of excessive computer storage, long computing time, and stability of numerical calculation. These mesh-related difficulties are associated with either finite-difference or finite-element methods. Spectral methods can be extremely accurate, but they have been used only with very simple geometries.

Recently, the vortex method has been developed[1,2] for the purpose of simulating two-dimensional incompressible and separated flows at high Reynolds numbers. In this numerical method, the vorticity is split into a large collection of vortices whose motion is tracked in time using a grid-free vortex tracing algorithm. Near-wall effects of viscosity are accounted for by the creation of discrete vortex sheets at the boundaries of the airfoils consistent with the no-slip condition. These boundary vortices then are released into the flowfield downstream of separation points obtained from a boundary-layer routine. For a cascade, periodicity along the cascade plane is imposed over a small integer number of blade passages. Using this method, detailed propagating stall computations were presented in Refs. 3 and 4 for a variety of nonvibrating cascades where the effects of camber and imposed wavelength were studied and an effort was made to parameterize the physical effects on stall propagation.

In those calculations, the airfoils were considered to be stationary. In fact, the blades of axial-flow turbomachinery may be excited to vibrate in various modes of bending and torsional vibration. There is strong interaction between the aerodynamics and the vibration, especially when stall or flow separation occurs, thus defining the aeroelastic nature of the problem. The purpose of the present work is to study propagating stall as it occurs in a cascade of airfoils vibrating in bending or torsion and how the vibration modifies the character of stalling. Based upon the method suggested in Ref. 1, the following modifications were incorporated into the present study:

1) When the blades vibrate, the adjacent flowfield is in motion. The boundary condition is therefore different from that of a stationary cascade, and the nonpenetration boundary condition must account for the motion of the airfoils.

2) Because the vibration of the blades are not in phase when propagating stall is present, the locations of the blades relative to each other vary with time. This affects the principal vortex-method matrix whose elements depend upon the distances between the wall points and are therefore time dependent. In general, this matrix would have to be updated and inverted at each time step. The cost would be exceedingly high. To reduce the needed computational time, a "piecewise linearization and recorrection technique" was developed in Ref. 5 for application to the present problem.

In this paper, the applicability of the vortex method to cascades of oscillating airfoils is assessed by first computing the unsteady incompressible lift, drag, and moment for small incidence, thickness, and vibratory displacement. These results are shown to be in excellent agreement with the available analytical results[6,7] for this so-called "classical" case. The data are for a limited sampling of cascade geometries, vibration amplitudes, reduced frequencies, and interblade phase angles. Flowfield data, including instantaneous streamline patterns and discretized vorticity distribution, are also presented as an aid to understanding.

Subsequently, a study is made of the effect of increasing the mean incidence up to and beyond the stall. Parametric studies of the effect of amplitude of vibration and stagger angle are reported. Important new results are presented showing the evolution of the classical reactions into the stalled flow reactions with mean incidence, oscillation frequency, and amplitude of vibration. In particular, the interaction between the structural response and the output aerodynamic reaction is demonstrated. Reference 8 presents some measurements of the blade vibration interaction with unsteady stalled flow, and in Ref. 9 the mechanism of stall flutter in cascaded airfoils is discussed.

The computations underlying the sample results are based on a modified form of the vortex method proposed by Spalart[1,2] to include blade motion. In its present form, the code requires the specification of the complete vibration mode and interblade phase angle at the outset of the computation. The implications for future direction of research and subsequent design code implementation are discussed.

Basic Aerodynamics Relations

For two-dimensional, viscous, incompressible flow past an infinite linear cascade of airfoils at high Reynolds number, the basic aerodynamic equations that govern the vorticity field derived in Ref. 1 are as follows:

Vorticity diffusion in the fluid:

$$D_t\omega = \nu\nabla^2\omega \tag{1}$$

where

$$\omega = \partial_x u - \partial_y v \tag{2}$$

Vorticity within the solid:

$$\omega = 2\Omega_m \tag{3}$$

The boundary conditions in terms of vorticity can be written as[1]

$$\oint_{s_m} (\nu\partial_n\omega)\, ds = -2R_m\, d_t\Omega_m \tag{4}$$

The system of equations governing the vorticity and the system governing the velocity and pressure field are equivalent. A stream function ψ can be defined as

$$u = -\partial_y\psi \text{ and } v = \partial_x\psi \tag{5}$$

which satisfies the continuity equation. Combining Eqs. (2) and (5) yields

$$\nabla^2\psi = \omega \tag{6}$$

The vortex method represents the vorticity field as the sum of a large number N of vortex blobs

$$\omega = \sum_{k=1}^{N} \omega_k \tag{7}$$

and the stream function induced by a collection of vortices is $\Sigma\psi_k$, where

$$\psi_k = -(\Gamma_k/4\pi)\, \ell_n\{|\sin[(2\pi i/p)(z - z_k)]|^2 + \xi^2\} \tag{8}$$

The other relations are the same as those in Refs. 1-3.

Vibration of Blade

For axial-flow turbomachinery, the sections of the blade usually are stacked with their centroids on a radial line. The blades may vibrate harmonically in each of several modes of bending and torsion. The bending is predominantly normal to the chord line of the airfoil, and the torsion occurs around its center of torsion as shown in Fig. 1. The offset of the center of twist from the centroid accounts for elastic and inertial coupling of the bending and torsional modes. The blade twist[10] accounts for additional coupling and for small chordwise bending displacements. In many engineering applications, bending and torsion amplitudes are relatively small, say, a few percent of chord for bending and at most a few degrees for torsion. The instantaneous coordinates of the airfoil sur-

face $[x(t),y(t)]$ under coupled bending and torsion are given by

$$x(t) = x_0 - h\sin(2\pi ft + \beta + m\sigma)\sin\zeta - y_0\theta\sin(2\pi ft + m\sigma) \quad (9a)$$

$$y(t) = y_0 + h\sin(2\pi ft + \beta + m\sigma)\cos\zeta + x_0\theta\sin(2\pi ft + m\sigma) \quad (9b)$$

where (x_0,y_0) are coordinates for each blade if they were rigid and are measured from its centroid, assumed here to coincide with the center of twist. The quantity β refers to the intrablade phase angle, which is equal to the phase difference between the bending and torsional modes and is set to zero in the present analysis. On the other hand, the interblade phase angle σ represents the phase shift between neighboring blades. At the airfoil surfaces, the nonpenetration condition is imposed, which requires that the normal velocity of the fluid at the body surface equal the normal velocity of the body. From the instantaneous coordinates of the airfoils, the normal vector $\boldsymbol{n}$ at each point can be evaluated at each time step. Since

$$\boldsymbol{V}\cdot\boldsymbol{n} = \boldsymbol{V}_b\cdot\boldsymbol{n} \quad (10)$$

and the relation $\partial_s\psi = V_n$, where s and n are the local coordinates parallel and normal to the wall, respectively, the incremental value of stream function along the airfoil surface can be determined from

$$d\psi|_s = \int_{s_0}^{s_0+\Delta s} V_n\,ds = \int_{s_0}^{s_0+\Delta s} (u_b n_x + v_b n_y)\,ds \quad (11)$$

This equation is used to determine the stream function distribution along the boundary points of the blades and thus to form the boundary conditions needed to solve the vorticity-stream function equation. As a consequence of the blade motion, the stream function is not constant along the boundary of the airfoils. It should also be emphasized that the no-slip condition is satisfied in a weak sense, as discussed in Ref. 1. Periodicity along the cascade is enforced by treating a small integral number of blade passages (1–6 usually).

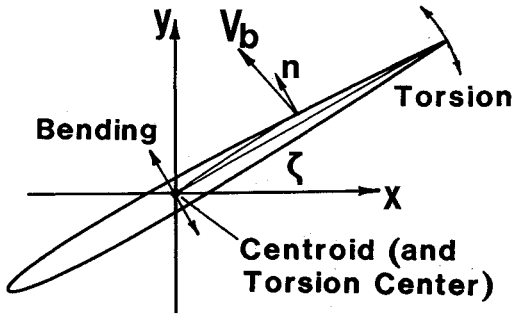

Fig. 1 Physical configuration and coordinate system.

Unsteady Lift, Drag and Moment Coefficients

Analytical methods for calculating the aerodynamic forces and moments acting on unstalled vibrating cascade with small incidence, thickness, and vibratory displacement, the so-called "classical" case, were suggested by Sisto[6] and Whitehead[7] among others.

The applicability of the vortex method to cascades of oscillating airfoils is assessed by first computing the unsteady incompressible lift, drag, and moment coefficients for the "classical" case. For comparison, computations were made for an unstaggered cascade of NACA-0008 airfoils vibrating in bending and with unit solidity and zero mean incidence (in conformance with these previous investigations). Several values of reduced frequency, vibration amplitude, and interblade phase angle were considered.

In the analytical investigations, the fluid is assumed to be inviscid. In the present work, the outer flow is also assumed to be inviscid; however, the flow near the airfoil surface is endowed, in a sense, with viscosity. A Reynolds number is specified, and the separation points are determined from a boundary-layer analysis. The results are found to be sensitive to the separation point locations. For a valid comparison with the analytical solution, the separation points are fixed near the trailing edge of the airfoils in the ensuing computations. Because of computer limitations, the maximum number of vortices was fixed at 500, and the number of bound vortex points was kept at 50. A vortex merging algorithm was used to keep the total number of vortices nearly constant with time.

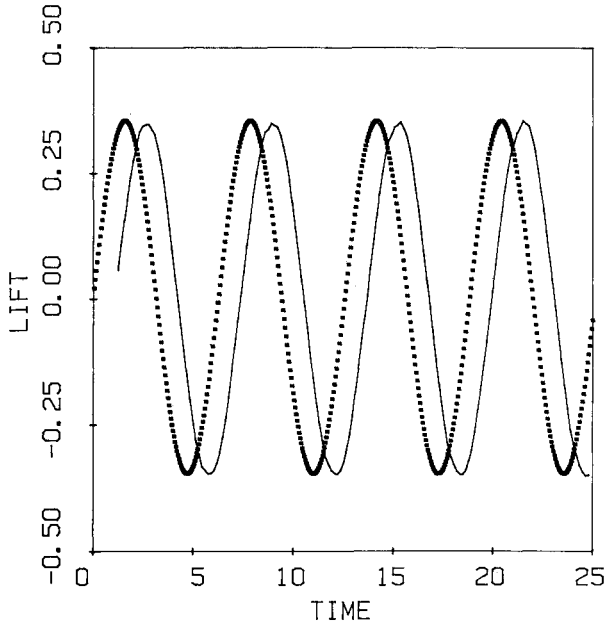

Fig. 2 Variation of lift coefficient with time; $K = 0.5$, $\sigma = 0$, $h = 0.05$, $\zeta = 0$ deg, $\alpha = 0$ deg (data have been averaged over three consecutive time steps).

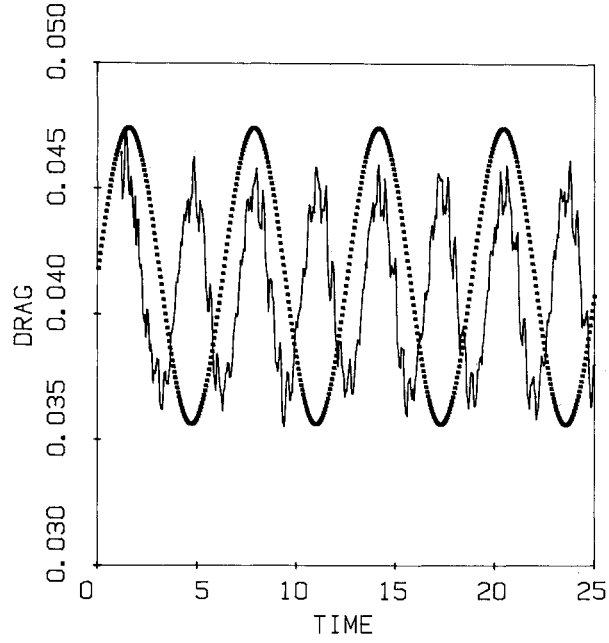

Fig. 3 Variation of drag coefficient with time (other parameters are same as in Fig. 2).

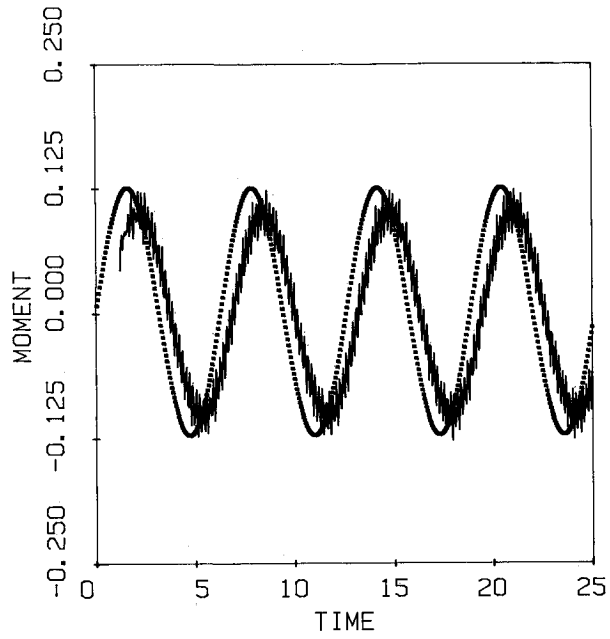

Fig. 4 Variation of moment coefficient with time (other parameters are same as in Fig. 2).

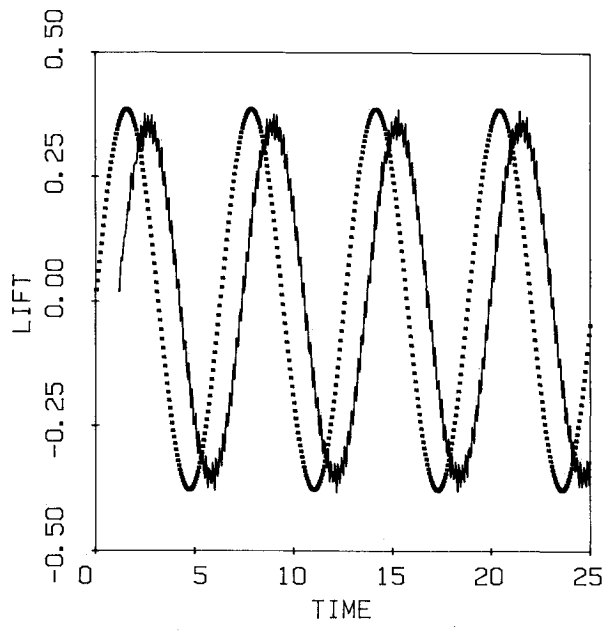

Fig. 5 Variation of lift coefficient with time (data include noise; other parameters same as in Fig. 2).

Typical numerical results for the unsteady lift, drag, and moment coefficients are shown in Figs. 2-4. In Fig. 2, the unsteady lift coefficient oscillates at the same frequency as the blade vibration. The dotted line is the displacement of the vibrating blade (scale not shown), so that the phase angle between the lift and displacement can be illustrated. The drag coefficients also oscillate, but with twice the vibrating frequency. This is reasonable, since the drag should vary with the frequency of the absolute value of the displacement. The drag is negative in the mean, i.e., it is actually a thrust. This is in keeping with the propulsive effect generated by oscillating airfoils. The order of magnitude appears to be correct, but the predicted drag is not accurate enough for quantitative comparison with theory, especially for low frequencies.

One observes some noise in the computed aerodynamic reactions due, most likely, to the following factors: 1) the maximum number of vortices allowed is not sufficient for computational stability, especially for low frequencies; 2) the numerical results are very sensitive to the selected method for merging vortices after each time step (this is the topic of discussion in another paper); and 3) as noted in Ref. 5, noise introduced by the piecewise linearization and recorrection technique can be smoothed by averaging. The coefficients of lift plotted in Fig. 2 were obtained by averaging over three consecutive time steps. For comparison, the unaveraged data for a frequency of $K = 0.5$ is also shown in Fig. 5.

Table 1 shows the present results to be in excellent agreement with the available analytical results[6,7] for various reduced frequencies, interblade phase angles, and bending amplitudes. Except for one case, the difference between the analytical and numerical results, including both amplitude and phase angle, is less than 5%. The computed lift coefficient of the adjacent blades are compared in Fig. 6. Obviously, the phase angle between the lift coefficients is equal to the interblade phase angle of vibration, in this case $2\pi/3$.

Streamline Patterns and Vorticity Distribution

Additional flowfield data, not easily accessible from a purely analytical approach, also are presented as an aid to understanding. These are the streamline patterns and the spatial distribution of the vortices. It should be emphasized that a streamline in an absolute frame of reference in general need

Table 1a Comparison of unsteady lift coefficient due to plunging for zero stagger, zero mean incidence at various interblade phase angles σ, and reduced frequencies K (amplitude of vibration = 5% of chord)

		Amplitude of lift coefficient		Phase of lift coefficient	
σ	K	Analytical[a]	Vortex method[b]	Analytical	Vortex method
0	1.00	0.4747	0.4770	−2.2574	−2.3673
0	0.50	0.3542	0.3586	−2.5994	−2.5426
0	0.25	0.3167	0.3126	−2.8500	−2.9671
0	0.10	0.3067	0.3102	−3.0223	−3.0065
π	1.00	0.8254	0.8225	−2.6608	−2.6672
π	0.50	0.8756	0.9060	−3.1600	−3.3011
π	0.25	1.1081	1.2043	−3.2924	−3.2921
π	0.10	1.2757	1.4900	−3.2334	−3.2465
0	1.00	0.4747	0.4770	−2.2574	−2.3673
π	1.00	0.8254	0.8225	−2.6608	−2.6672
$2\pi/3$	1.00	0.7644	0.7855	−2.6154	−2.6840
0	0.50	0.3542	0.3586	−2.5994	−2.5426
π	0.50	0.8756	0.9060	−3.1600	−3.3011
$2\pi/3$	0.50	0.7760	0.7919	−3.1310	−3.1171
$-2\pi/3$	0.50	0.7760	0.7919	−3.1310	−3.1171

[a]Obtained from the spectral analysis of lift data. [b]Obtained from Ref. 6.

Table 1b Comparison of unsteady lift coefficient showing the effect of vibration amplitude (other conditions same as Table 1a)

			Amplitude of lift coefficient		Phase of lift coefficient	
σ	K	Amplitude, % chord	Analytical[a]	Vortex method[b]	Analytical	Vortex method
$2\pi/3$	1.0	5	0.7644	0.7855	−2.6154	−2.6840
$2\pi/3$	1.0	10	0.7644	0.7881	−2.6154	−2.6840
π	0.5	5	0.8756	0.9060	−3.1600	−3.3011
π	0.5	10	0.8756	0.9238	−3.1600	−3.3011
π	0.5	20	0.8756	0.9208	−3.1600	−3.3011

[a]Obtained from the spectral analysis of lift data. [b]Obtained from Ref. 6.

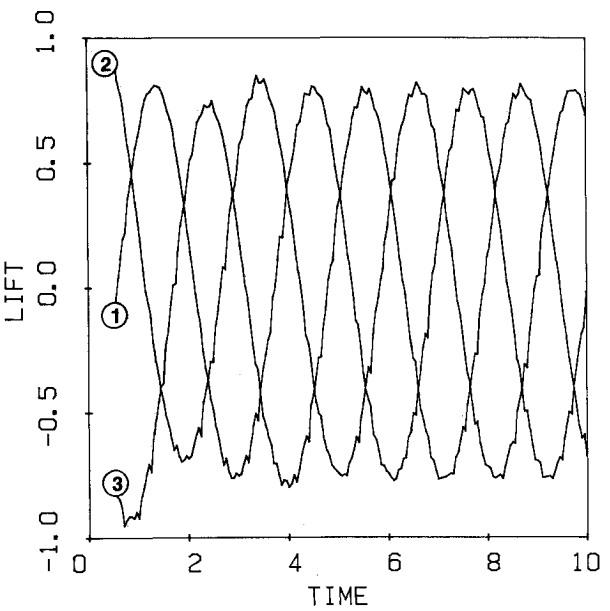

Fig. 6 Displacement histories showing the phase angle between the lift coefficient of adjacent blades; $K = 1.0$, $\sigma = 2\pi/3$, $h = 0.05$, $\zeta = 0$ deg, $\alpha = 0$ deg.

Table 2 Lift response vs inlet flow angle (for $K = 0.5$, $\sigma = \pi$, $h = 0.05$, $\zeta = 0$ deg)

Incidence, deg	Vortex method[a]		Analytical[b]	
	Amplitude	Phase	Amplitude	Phase
0	0.9393	−3.2805	0.8756	−3.1600
20	0.9102	−3.1942	—	—
40	0.6701	−3.3616	—	—
45	1.1048	−2.7653	—	—
50	2.6902	−2.4949	—	—
55	2.9234	−1.2716	—	—

[a]Obtained from spectral analysis of lift data. [b]Obtained from Ref. 6.

not lie along the surface of a blade when the blade is in motion.

As shown in Figs. 7a and 7b, when the mean incidence is small, the streamline pattern does not indicate stall. At higher incidence, the occurrence of stall is clearly evident as in Fig. 8 and the period of its propagation can be obtained by comparing the streamline patterns at different times. It is interesting to observe that free vortices pattern is distinctly oscillatory and asymmetrical with respect to the blade chord downstream extension, as shown in Figs. 9 and 10. In particular, the phenomenon is rather obvious for high frequencies. The oscillatory velocity of the blade, as well as the strength and transport velocity of the free vortices, will increase with the frequency of vibration, so that the amplitude of the sinuous wake formed by the free vortices also will increase with frequency.

In all these studies, as well as those to follow, the importance of the interblade phase angle as a governing parameter is strongly evident.

Effect of Mean Incidence

One of the objectives of this study is to chart the evolution of unsteady separation in a cascade of vibrating blades as the mean incidence is increased toward stall. In a series of studies, the mean incidence for a cascade of zero stagger is increased from 0-55 deg in five increments. The cascade geometry is unchanged, and the reduced frequency ($=0.5$) and interblade phase angle ($=\pi$) are held fixed. The corresponding numerical results are presented in Table 2.

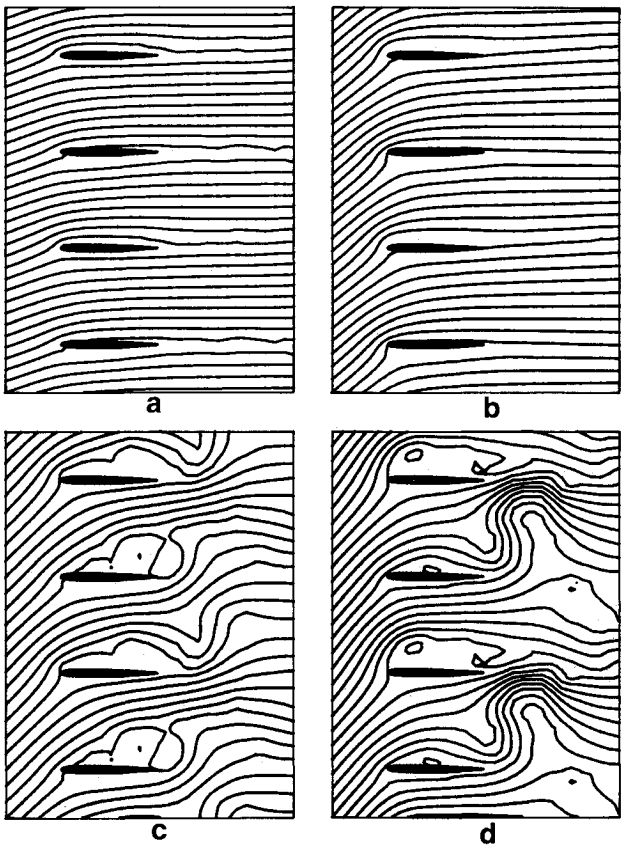

Fig. 7 Instantaneous streamline patterns for different mean angles of incidence $K = 0.5$, $\sigma = \pi$, $h = 0.05$, $\zeta = 0$ deg; a) $\alpha = 20$ deg, $t = 24.75$; b) $\alpha = 40$ deg, $t = 80.50$; c) $\alpha = 45$ deg, $t = 80.50$; d) $\alpha = 50$ deg, $t = 80.50$.

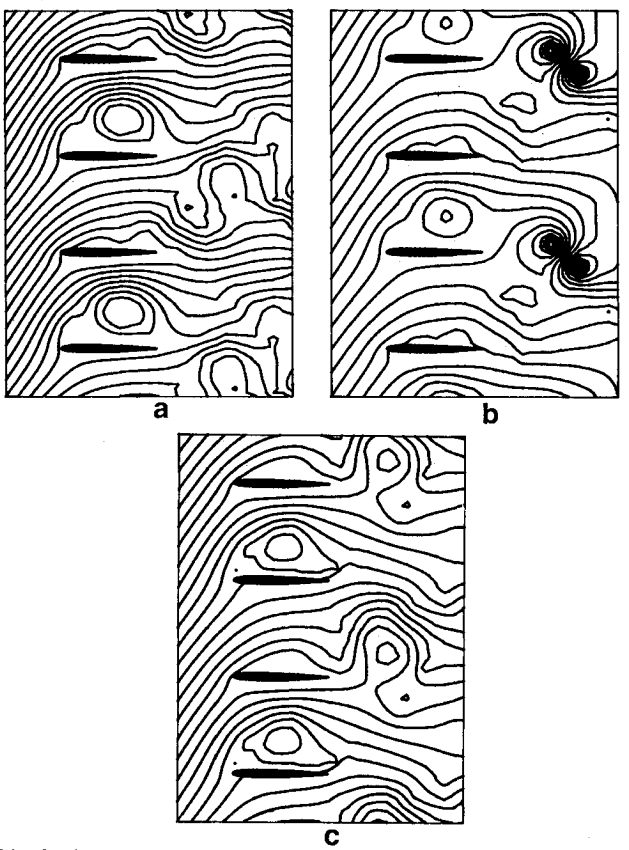

Fig. 8 Streamline pattern in stall flutter regime for plunging oscillation at different time levels; $K = 0.5$, $\sigma = \pi$, $\zeta = 0$ deg, $\alpha = 55$ deg, period of vibration ($t_v = 1/f = 6.28$): a) $t_a = 240.75$; b) $t_b = 243.75$ ($\sim t_a + t_v/2$); c) $t_c = 246.75$ ($\sim t_a + t_v$).

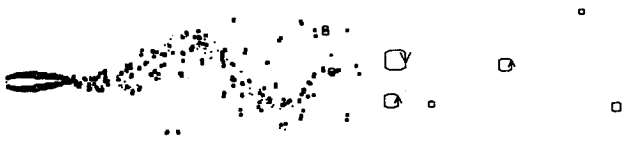

Fig. 9 Distribution of vortices at time $t = 15$; $K = 1.0$, $\sigma = 0$, $h = 0.05$, $\zeta = 0$ deg, $\alpha = 0$ deg (the size of the vortex represents its strength; for larger vortices, the direction of rotation is shown by the arrows).

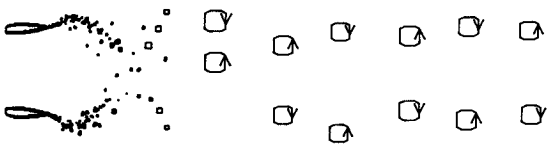

a) Torsion: $K = 1$, $\sigma = \pi$, $\theta = 5$ deg, $\zeta = 0$ deg, $\alpha = 0$ deg

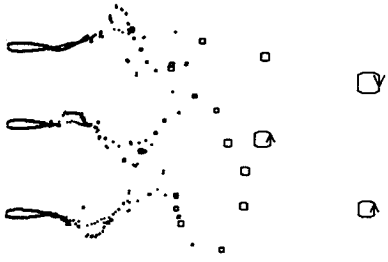

b) Bending: $K = 1$, $\sigma = 2\pi/3$, $h = 0.05$, $\zeta = 0$ deg, $\alpha = 0$ deg

Fig. 10 Distribution of vortices at time $t = 25$.

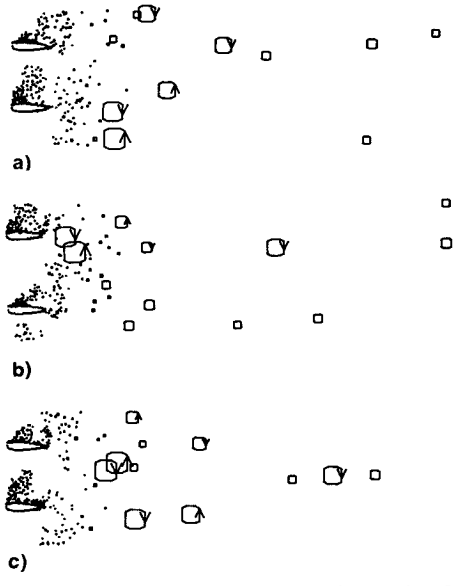

Fig. 11 Distribution of vortices corresponding to time levels shown in Fig. 8 (the size of the vortex represents its strength; for larger vortices, the direction of rotation is shown by the arrows).

Typical streamline patterns are shown in Figs. 7 and 8. Obviously, for low incidence of 0 and 20 deg, the stall does not occur. Stall occurs if the incidence is increased to about 40 deg (Fig. 7c). In Fig. 8, propagating stall is illustrated, and the dimensionless period of propagation, 6.0, is close to the impressed dimensionless period of vibration, 6.28. The distributions of vortices corresponding to the three successive times

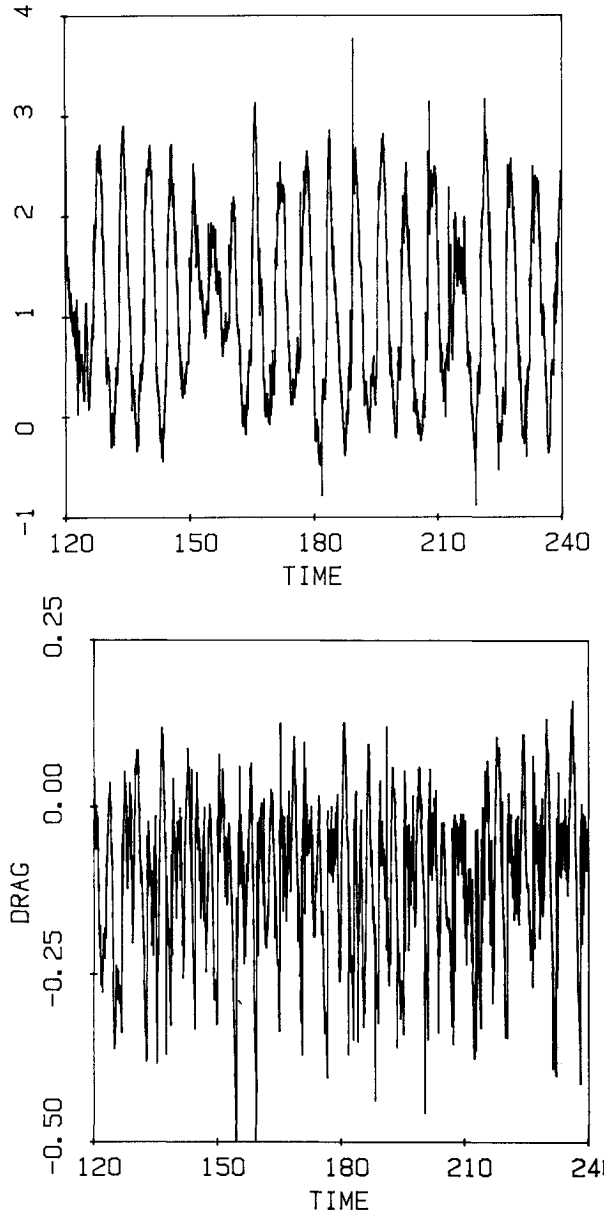

Fig. 12 Lift and drag coefficients as a function of time in the stall regime (other parameters are the same as in Fig. 10).

shown in Fig. 8 are plotted in Fig. 11 and display a similar periodic variation. The periodic structure also can be observed in a plot of the lift coefficient with the time, as shown in Fig. 12. The lift coefficient does not seem to be a simple sinusoidal variation, as in the unstalled cases shown in Fig. 2. In the lift coefficient, there are frequency components that correspond to the propagating stall phenomenon and components corresponding to the blade vibration frequency. This important characteristic is demonstrated quantitatively in the following section.

Spectral Postprocessing

The object of frequency analysis is to decompose a complex signal into its harmonic components. Fourier transforms of the computed unsteady lift and drag coefficients were obtained, yielding the variation of these coefficients as a function of frequency.

For the incidence study mentioned earlier, the spectrum of the lift and drag coefficient for 55 deg incidence are shown in Figs. 13–16. As expected, there are lift responses due to stall propagation whose frequencies are different from the fre-

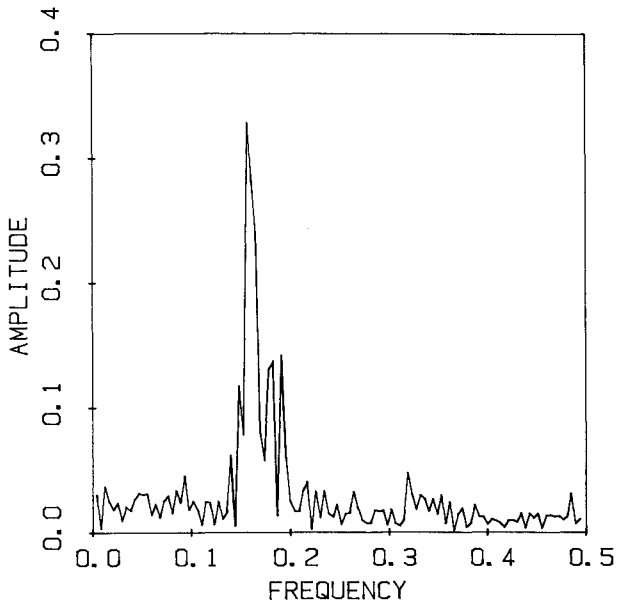

a) Spectrum for lift

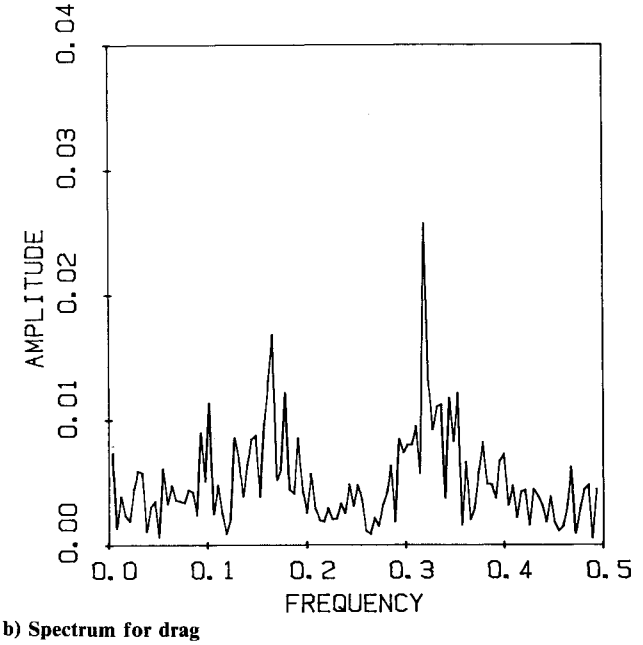

b) Spectrum for drag

Fig. 13 Effect of vibration amplitude; $K = 0.5$, $\sigma = \pi$, $h = 0.05$, $\zeta = 0$ deg, $\alpha = 55$ deg.

quency of the lift response impressed by blade motion. Furthermore, comparing the spectrum of the drag coefficient with that of the lift coefficient, the frequency of the peak drag is seen to be double that of lift. This is consistent with the analysis mentioned above.

Effect of Vibration Amplitude

In the spectra, for example as shown in Fig. 13, there are two peaks. One peak, whose nondimensional frequency is approximately 0.157, is the lift response caused by the vibration of the blade, which occurs at a frequency of 0.159 (reduced frequency is 0.5). Another peak at a frequency of 0.191 is the characteristic "response" caused by stall propagation. It should be noted that since the propagating stall phenomenon is essentially an instability of the flow; its structure can be considered to be an eigenfunction of a nonlinear system, and the stall frequency is the "characteristic value." In order to observe the relative variation of the intensity of these two responses, an amplitude study was undertaken. In this study, the dimensionless amplitude of vibration is decreased from

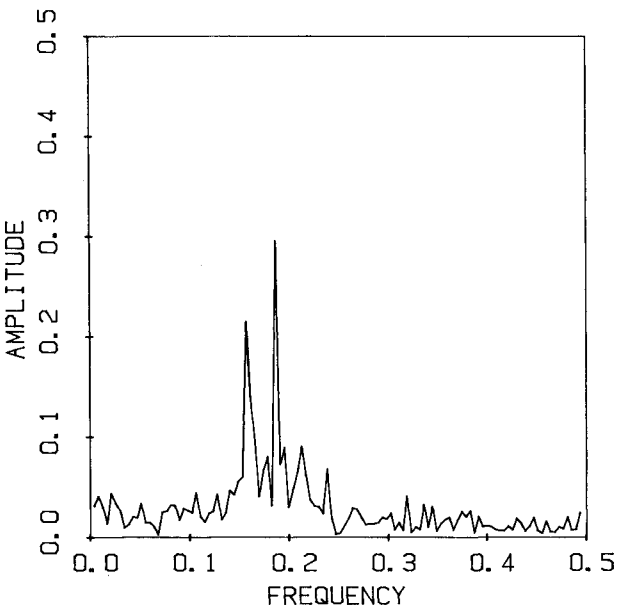

Fig. 14 Effect of vibration amplitude: spectrum for lift with $h = 0.03$ (other parameters same as in Fig. 13).

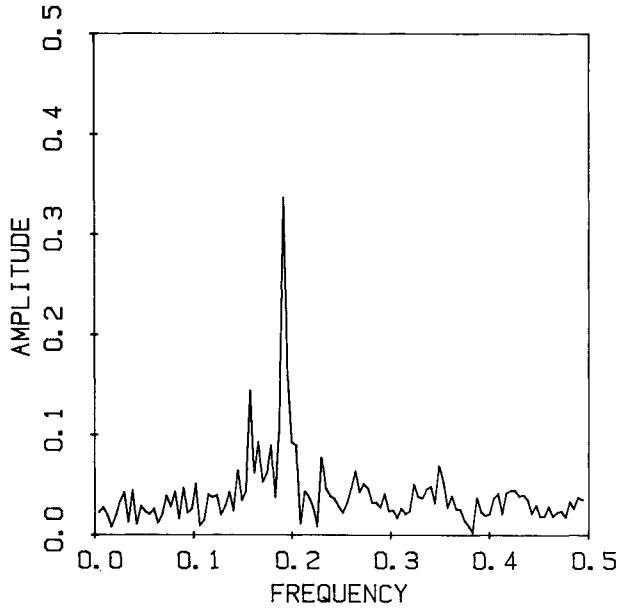

Fig. 15 Effect of vibration amplitude: spectrum for lift with $h = 0.02$ (other parameters same as in Fig. 13).

Table 3 Peak response from lift spectra showing decrease in lift amplitude at propagating stall frequency and increase in life amplitude at vibration frequency

Vibration amplitude	Lift response due to vibration		Lift response due to propagating stall	
	Frequency	Amplitude	Frequency	Amplitude
0	—	—	0.193	0.360
0.02	0.157	0.148	0.191	0.340
0.03	0.157	0.216	0.187	0.295
0.05	0.157	0.460	0.191	0.130

0.05 to 0.03, 0.02, and 0 consecutively, while the other parameters are held fixed. Here, zero amplitude implies that the blades are held fixed so that only propagating stall may be expected.

The lift spectra obtained for different amplitudes of vibration appear in Figs. 13–16. By studying these figures and the results shown in Table 3, the following conclusions can be

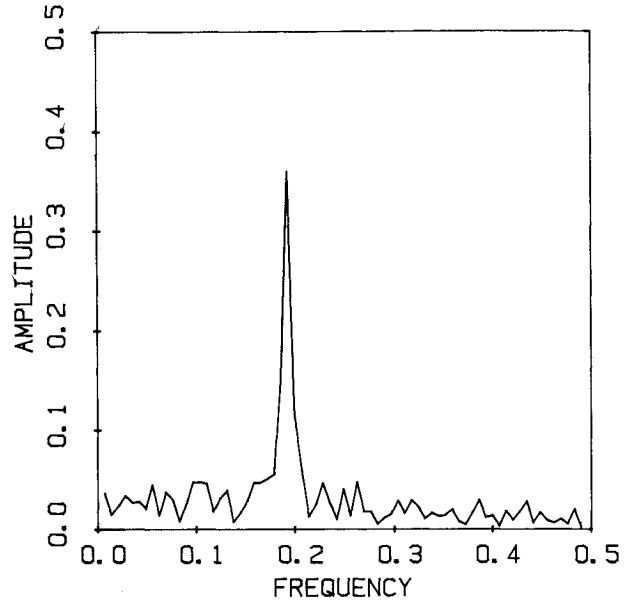

Fig. 16 Effect of vibration amplitude: spectrum for lift with $h = 0.0$ (other parameters same as in Fig. 13).

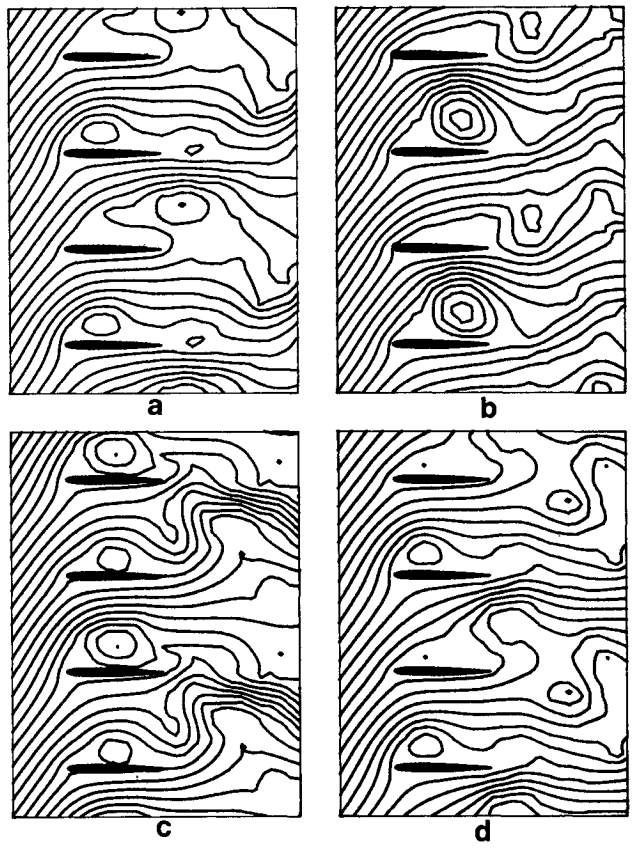

Fig. 17 Streamline patterns for the case shown in Fig. 16 at different times: a) 150.75; b) 152.50; c) 154.25; d) 156.00.

drawn:

1) The frequencies of the peaks in response to blade vibration and to propagating stall, respectively, do not change as the amplitude of vibration is decreased from 0.05 progressively to zero.

2) When the blades are held fixed, there is only one peak in the spectrum, and it is attributable to propagating stall.

3) The smaller the amplitude of vibration, the smaller is the corresponding spectral response.

4) Lift response at the propagating stall frequency decreases as the vibration amplitude increases.

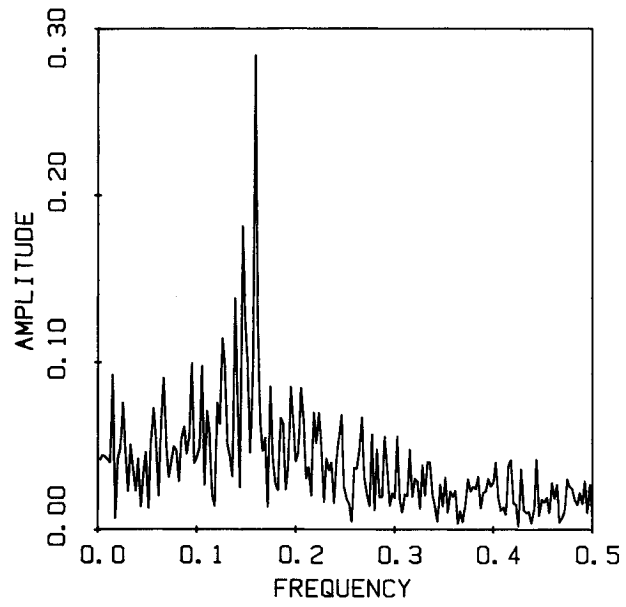

Fig. 18 Stagger angle study: spectrum for lift; $K = 0.5$, $\sigma = \pi$, $h = 0.02$, $\zeta = 20$ deg, $\alpha = 75$ deg.

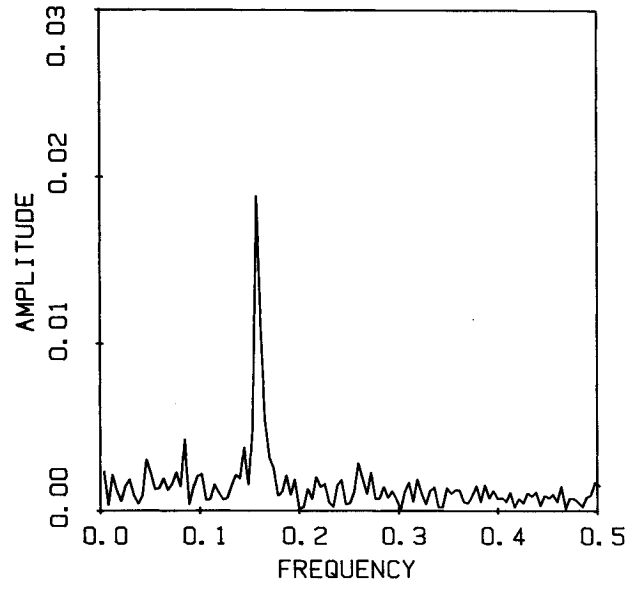

Fig. 19 Stagger angle study: spectrum for lift; $K = 0.5$, $\sigma = \pi$, $h = 0.02$, $\zeta = 45$ deg, $\alpha = 75$ deg.

These characteristics are also confirmed by observing the streamline patterns. For example, in Fig. 8, the period of propagation determined by tracking the stall patch in time is equal to the period of vibration. This may be understood from the fact that in this case the amplitude of vibration, 0.05, is rather large and is sufficient to induce the nonlinear phenomenon of entrainment of frequency. On the other hand, according to the spectrum analysis of the results obtained when the blades are held fixed, the period of propagation is 5.18 (i.e., inverse of 0.193), which is consistent with the analysis of the streamline patterns at the corresponding time steps shown in Fig. 17.

Stagger Angle Study

In order to assess realistic turbomachinery geometries, a stagger angle study was conducted. The inlet flow angle (75 deg) and the amplitude of vibration ($A = 0.02$) are held fixed, while calculations are presented for a stagger angle of 20 and 45 deg. The selected airfoil is a double-circular arc type with 10 deg camber and 10% thickness. Although the lift spectrum, shown in Fig. 18, is more complicated than those described

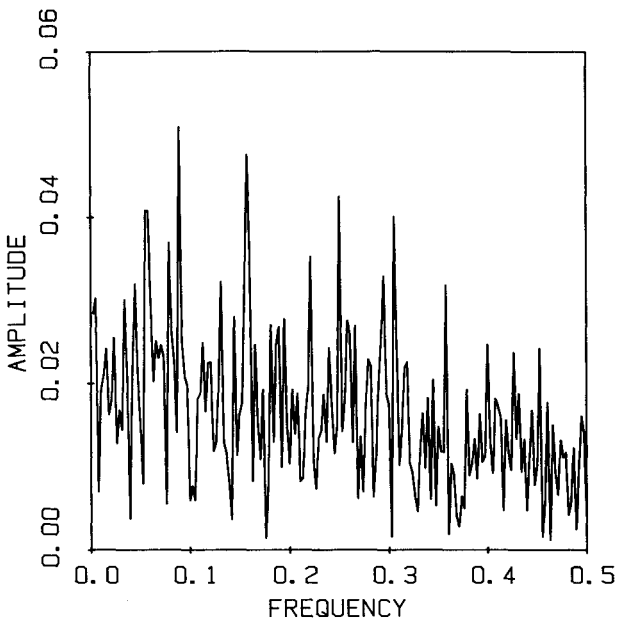

Fig. 20 Stagger angle study: spectrum for lift; $K = 0.5$, $\sigma = \pi$, $h = 0.05$, $\zeta = 45$ deg, $\alpha = 75$ deg.

previously, once again there are two peaks that are the responses to vibration and stall propagation. The frequency of response due to vibration is still near the specified frequency of vibration 0.159, but the frequency of response due to propagating stall is about 0.10, less than that for zero stagger. The intensities of the peaks are all weaker than the zero stagger angle example. For the 45 deg stagger calculation depicted in Fig. 19, the angle of incidence was effectively reduced by 25 deg. The boundary-layer model used in the present analysis failed to predict gross separation in this case so that the lift spectrum shows only the expected response at the impressed vibration frequency. This result was confirmed by an examination of the streamline pattern (not shown). If the amplitude of vibration is increased from 0.02–0.05, the spectrum is as shown in Fig. 20. The frequencies of the lift response peaks due to vibration and stall are not changed appreciably, but the intensity is increased.

Conclusions and Discussion

A numerical simulation has been presented for propagating stall in a linear cascade of vibrating blades using the vortex method.

The applicability of the vortex method to a cascade of airfoils in phased vibratory motion was assessed by first computing the unsteady incompressible lift, drag, and moment for small incidence, thickness, and vibratory displacement. These results are shown to be in excellent agreement with available analytical theories. Although the data are for a limited sampling of reduced frequencies, interblade phase angles, and vibration amplitudes, it was concluded that the vortex method as modified for oscillating cascaded airfoils can be applied reliably.

Additional flowfield data including the streamline pattern and the discretized vorticity distribution were also presented. In all the studies, the importance of the interblade phase angle as a governing parameter is strongly evident, whether in the streamline pattern, distribution of vorticity, or lift, drag, and moment response. Hence, the eventual aeroelastic application of the method must permit the natural development of the inherent interblade phase angle evolution.

A study was made of the effect of increasing the mean incidence up to and beyond the stall. A spectral decomposition of the unsteady lift and drag coefficients revealed important new results showing the evolution of classical reactions into the stalled flow reactions as function of mean incidence, amplitude of vibration, and stagger angle. In particular, the complicated interaction between the structural frequency of the blades (considered as one of the inputs to a nonlinear aeroelastic system) and the output frequency spectrum of the aerodynamic reactions is demonstrated. It has been confirmed by computation that the spectra of lift and drag responses to the imposed blade motion contain frequencies related to oscillation frequency as well as nonsynchronous frequencies associated with the inherent propagating stall frequency of the cascade. Furthermore, the frequency content may be expected to change with time as the initial transient response decays.

Quantitative analysis of the various responses yield not only the frequency but also the intensity and phase of the response. For example, when the amplitude of vibration is changed, the frequency content of the response usually does not change. In addition, the larger the amplitude of vibration, the larger the response to that vibration. More significant is the fact that the lift response at the propagating stall frequency decreases as the vibration amplitude increases, provided the two frequencies are distinct. Thus, the stall frequency effectively is entrained by the vibration for sufficiently high amplitudes of vibration. When entrainment does occur, due to strong fluid/structure coupling, the stall frequency becomes identical to the vibration frequency, and there is a single predominant frequency in the steady-state lift spectrum. When entrainment does not occur, two distinct frequencies may continue to be observed. In future applications, where the impressed blade motion is no longer specified and blades are elastically supported, it may be expected that the coupling will be more complex.

The vortex method is a very useful tool for understanding the complicated mechanism of unsteady cascade stall and may be expected to yield quantitatively useful results. On other hand, the illustrated computations are based on a program that still contains some deficiencies. The most egregious of these is that the mode, amplitude, frequency, and interblade phase angle must be specified. These restrictive assumptions or specifications were necessary in order to concentrate on the unsteady aerodynamic response. In fact, there is strong interaction between the structural response and the aerodynamics. However, these assumptions all may be removed in the future if the full aeroelasticity problem is analyzed with further development of the computational algorithm. The resulting code will necessarily contain two large subprograms, one describing the unsteady aerodynamics and the other concerning the structural dynamics of the cascade of blades. A large number of blades must be capable of being represented and both subprograms will be used during each time sequence. In this manner, no a priori assumption need be made concerning periodicity along the cascade. Most likely, a supercomputer will be required for efficient execution of such an extensive time-dependent problem. The vortex method, as used in these initial computational studies pointing toward the aeroelastic application, also will benefit from an improved boundary layer model. In particular, stall inception under dynamic conditions needs to be modeled more accurately.

Acknowledgments

This work was supported in part by the Office of Naval Research under Contract N00014-86K-0315 for which Dr. R. P. Shreeve of the Naval Postgraduate School served as the project monitor. The authors are indebted to Dr. P. R. Spalart for providing the computer code that served as the starting point of this investigation and to Dr. Paul Kutler for time made available on the CRAY-XMP/48 supercomputer at the NASA Ames Research Center. Acknowledgment is also made to Stevens Institute of Technology for the support of Prof. Wu and for use of the Institute's computer facility.

References

[1]Spalart, P. R., "Numerical Simulation of Separated Flows," NASA TM-84238, Feb. 1983.

[2]Spalart, P. R., "Two Recent Extensions of the Vortex Method," AIAA Paper 84-0343, Jan. 1984.

[3]Speziale, C. G., Sisto, F., and Jonnavithula, S., "Vortex Simulation of Propagating Stall in a Linear Cascade of Airfoils," *Transactions of ASME, Journal of Fluids Engineering,* Vol. 108, Sept. 1986, p. 304.

[4]Jonnavithula, S., Sisto, F., and Thangam, S., "Parametric Study of Propagating Stall in Linear Cascades," Paper presented at 39th Annual Meeting of the American Physical Society-Division of Fluid Dynamics, Columbus, OH, Nov. 1986.

[5]Wu, W., Sisto, F., Thangam, S., and Jonnavithula, S., "Vortex Simulation of Unsteady Stall in a Cascade of Oscillating Blades with Piecewise Linearization and Recorrection Technique," *Numerical Methods in Laminar and Turbulent Flow,* Vol. 5, edited by C. Taylor, W. G. Habashi, and M. M. Hafez, Pineridge Press, New York, 1987, pp. 1687–1697.

[6]Sisto, F., "Unsteady Aerodynamic Reactions of Airfoils in Cascade," *Journal of the Aeronautical Sciences,* Vol. 22, May 1955, p. 297.

[7]Whitehead, D. S., "Force and Moment Coefficients for Vibrating Aerofoils in Cascade," British Aeronautical Research Council, London, R&M 3254, 1960.

[8]Dowell, E. H., Curtiss, H. C., Jr., Scanlan, R. H., and Sisto, F., *A Modern Course in Aeroelasticity,* Sijtthoff & Noordhoff, Amsterdam, 1978.

[9]Huppert, M. C., Johnson, D. F., and Costilow, E. L., "Preliminary Investigation of Compressor Blade Vibration Excited by Rotating Stall," NACA RM-E52J15, Dec. 1952.

[10]Sisto, F. and Chang, A. T., "A Finite Element for Vibration Analysis of Twisted Blades Based on Beam Theory," *AIAA Journal,* Vol. 22, Nov. 1984, p. 1646.